J Mol Model (2014) 20:2539
DOI 10.1007/s00894-014-2539-3

ORIGINAL PAPER

Functionalization of the pristine and stone-wales defected BC_3 graphenes with pyrene

Ali Ahmadi Peyghan · Maziar Noei · Zargham Bagheri

Received: 3 May 2014 / Accepted: 17 November 2014 / Published online: 11 December 2014
© Springer-Verlag Berlin Heidelberg 2014

Abstract The functionalization of pristine and Stone-Wales defected BC_3 nanosheets with a pyrene molecule was investigated using density functional theory. Frontier molecular analysis shows that the main interaction is π-π stacking, releasing energies in the range of 143.6 to 169.1 kJ mol^{-1}. We predicted that after the functionalization process, the electrical conductance of the pristine sheet may be increased. Also, it modifies the work function of the pristine sheet and, as a consequence, its field-emission current densities may significantly enhance. However, the pyrene functionalization results in little change in the electronic properties of the defected sheet.

Keywords B3LYP · DFT · Functionalization · Graphene

Introduction

Since their discovery for the first time in experiments in 2004 [1], graphene and graphene-like materials have been under investigation theoretically and experimentally because of their novel physical and chemical properties [2–9]. Owing to the equivalence of two carbon sites, the graphene sheet is a semimetal with the massless Dirac-like electronic excitation [10]. Studies of as-grown graphene, radiation treated graphite, and other carbon nanostructures have revealed that defects are common phenomena in carbon-based nanomaterials. Therefore, understanding the properties of intrinsic or artificial defects has become essential for the further development of many applications, including nanoelectronic devices, intramolecular junction, and graphene-based sensors.

Typically, it is possible to tailor the desired bandgap for such a system via formation of nanoribbons by cutting a graphene sheet or by attaching foreign atoms to the pristine layer [11, 12]. These graphene sheets can be transformed into multidimensional carbon materials by self-assembly, so they are the (2D) building block for many carbon materials. Nevertheless, graphene usually suffers from various types of defect in the atomic structures during its growth. Boron atoms have been widely used as dopants in carbon nanostructures for building functional materials because of their similar atomic radius. Not surprisingly, a uniform BC_3 sheet (*h*-BC_3) has already been synthesized in the laboratory [13]. Its geometric structure was found to be almost identical to graphene, except that some carbon atoms are replaced by boron atoms so that six carbon atoms form a hexagon surrounded by six boron atoms [14, 15]. In addition, Pontes et al. found that boron atoms can substitute carbon atoms in a graphene sheet without any activation barrier [16]. However, it should be noted that the BC_3 honeycomb sheet is a semiconductor with an indirect gap, while graphene is a semiconductor with a zero gap. Theoretical works [17, 18] revealed that the tunable electronic properties of the BC_3 sheets are feasible.

Following the carbon nanotube (CNT) and graphene discovery, it was soon acknowledged that their poor solubility in polar solvents (which has implications in the formation of aggregates in aqueous solutions) is detrimental for biological applications. Functionalized CNT and graphene are typically easy to disperse in organic solvents and water. Therefore, the functionalization procedure can improve the dispersion and homogeneity of these compounds in the desired solvents [19,

A. A. Peyghan (✉)
Young Researchers and Elite club, Central Tehran Branch, Islamic Azad University, Tehran, Iran
e-mail: ahmadi.iau@gmail.com

M. Noei
Department of Chemistry, College of Chemical Engineering, Mahshahr Branch, Islamic Azad University, Mahshahr, Iran

Z. Bagheri
Department of Physics, College of Science, Islamshahr Branch, Islamic Azad University, Islamshahr, Iran

20]. The functionalization of nanostructures is achieved through covalent bonding or physical interaction of foreign species. It has been demonstrated that the covalent bonding of amino acids, hydroxyl and carboxyl groups, and so forth through the replacement of C-C bonds improves the CNT and graphene ability to interact with the biological environment [21].

An alternative nondestructive method for solubilization is based on non-covalent binding, as observed for CNT and graphene solubilization in organic compounds for which the weaker binding ability is described in terms of van der Waals interactions. Non-covalent functionalization is preferable for solubilization, because it enables attachment of aromatic molecules through π-π stacking or hydrophobic interactions, thus still preserving the intrinsic electronic properties of graphene and CNTs. Noncovalent sidewall CNT functionalization with aromatic organic molecules such as benzene has attracted increasing attention [22].

Recently, theoretical calculations have also shown that BC_3 nanotubes (BC_3NTs) can be functionalized by various groups (such as ethylene [23] and lithium [24]), but there is no report in the literature about functionalization of BC_3 sheets. In this work, the interaction of pyrene ($C_{16}H_{10}$) with a pristine and a Stone-Wales defected BC_3 sheet have been theoretically investigated based on the analysis of structure, energies, electronic structures, stability, etc. Alternatively the soft computing methods such as genetic programming can also be further applied to investigate the electronic properties of these materials [25–29]. Pyrene (Fig. 1) is a polycyclic aromatic hydrocarbon (PAH) consisting of four fused benzene rings, resulting in a flat aromatic system. The chemical formula is $C_{16}H_{10}$. This colorless solid is the smallest peri-fused PAH (one where the rings are fused through more than one face).

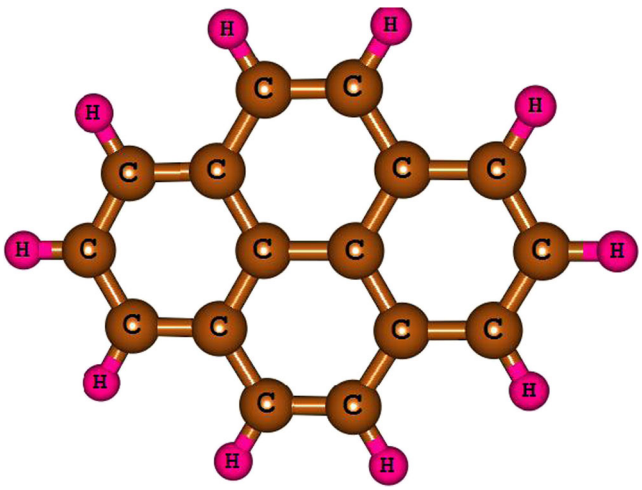

Fig. 1 Optimized structure of free pyrene

Computational methods

We selected BC_3 sheets which consisted of 102 C and 34 B atoms, in which the end atoms have been saturated with hydrogen atoms to reduce the boundary effects. The full geometry optimizations and property calculations were performed using three parameter hybrid generalized gradient approximation with the B3LYP functional augmented with an empirical dispersion term (B3LYP-D) with 6-31G basis set including the d-polarization function (denoted as 6-31G(d)) as implemented in the GAMESS suite of program [30]. To improve the description of the long-range interaction, we have employed the DFT-D [31] method of Grimme. In this approach, the total energy is calculated as a function of the dispersion coefficient for each atom pair, a global scaling factor that depends only on the exchange-correlation functional used, and a damping function to avoid near singularities for small distances. GaussSum program [32] has been used to obtain the density of states (DOS) results. The B3LYP density functional has been previously shown to reproduce experimental properties and has been commonly used in nanostructure studies [33–35]. We have defined the adsorption energy in the usual way as:

$$E_{ad} = E\,(BC_3\text{sheets}) + E\,(\text{pyrene}) - E\left(\text{pyrene}\Big/BC_3\text{sheets}\right) + E_{BSSE}, \quad (1)$$

where E (pyrene/BC_3 sheets) corresponds to the energy of the BC_3 sheets in which the pyrene has been adsorbed on the surface, E (BC_3 sheets) is the energy of the isolated sheet, E (pyrene) is the energy of a single pyrene molecule, and E_{BSSE} is the energy of the basis set superposition error. By definition, a positive value of E_{ad} corresponds to exothermic adsorption. To investigate the electronic charge changes through the BC_3 sheets, the net charge-transfer (Q_T) between pyrene molecule and the sheet is calculated by using natural bond orbitals (NBO) analysis which is defined as the charge difference between the pyrene molecule adsorbed on the BC_3 sheets and an isolated pyrene molecule. The canonical assumption for Fermi level (E_F) is that in a molecule (at T= 0 K) it lies approximately in the middle of the highest occupied molecular orbital (HOMO) and the lowest unoccupied molecular orbital (LUMO) energy gap (E_g). It is noteworthy to mention that, in fact, what lies in the middle of the E_g is the chemical potential, and since the chemical potential of a free gas of electrons is equal to its Fermi level as traditionally defined, herein, the Fermi level of the considered systems is at the center of the E_g.

Results and discussion

Geometry

A partial structure of the optimized BC_3 sheet in Fig. 2a shows that two types of bonds, including B-C, and C-C can be identified, with corresponding lengths of 1.56, and 1.42 Å, respectively. In order to find the adsorption behavior of a pyrene molecule on the sheet, it was placed on the top of the sheet as parallel, vertical, and diagonal to the sheet surface. We have considered the most stable configuration, in which the pyrene molecule is as near as possible to the BC_3 sheets (Fig. 2b). More detailed information, including values of E_{ad}, electronic properties and the charge transfer (Q_T), is listed in Table 1. In this case, the molecule is oriented in such a way that the pyrene surface is exactly parallel to sheet surface and π-π stacking interaction occurred. The distances from the sheet to the hexagon rings of the molecule are in the range of 2.89–3.00 Å, with corresponding E_{ad} of 169.1 kJ mol^{-1}. Figure 3 displays the HOMO of the pyrene/BC_3 sheets complex to illustrate the π-π interaction between the molecule and the sheet. The π-π interaction is a noncovalent attractive force between the aromatic rings. The alignment of the positive electrostatic potential on one ring with negative electrostatic potential on another ring forms an offset stack just like pyrene/BC_3 sheets complex. NBO analysis indicates the transfer of 0.220 electrons in the complex from the pyrene to the BC_3 sheets. As shown in a previous study [36], the B atoms are positively charged so that BC_3 sheets can act as electron-deficient partners, while pyrene is an electron-rich molecule. This phenomenon successfully demonstrated the direction of charge transfer from the molecule to the host sheet.

Table 1 Calculated adsorption energy (E_{ad}, kJ mol^{-1}), HOMO energies (E_{HOMO}), LUMO energies (E_{LUMO}), Fermi level (V) work function (Φ), and HOMO-LUMO energy gap (E_g) of systems in eV

Φ	E_g	E_{LUMO}	E_{FL}	E_{HOMO}	E_{ad}	System
1.33	2.67	−3.74	−5.07	−6.41	–	*h*-BC_3
1.09	2.19	−3.68	−4.77	−5.87	169.1	Pyrene/*h*-BC_3
1.08	2.16	−3.96	−5.04	−6.12	–	SW-CC
1.02	2.05	−3.76	−4.78	−5.81	167.7	CC.1
1.02	2.04	−3.78	−4.80	−5.82	165.3	CC.2
1.01	2.02	−3.86	−4.87	−5.88	164.1	CC.3
1.09	2.18	−3.74	−4.83	−5.92	–	SW-BC
1.04	2.09	−3.68	−4.72	−5.77	143.6	BC.1
1.07	2.14	−3.67	−4.74	−5.81	162.9	BC.2
0.97	1.94	−3.71	−4.68	−5.65	164.6	BC.3

The typical topological defect in the nanostructures is the SW defect which consists of two pairs of five-membered and seven-membered rings. The SW defect can be created by rotating a bond by about 90°. Two types of SW defects for the BC_3 sheets (labeled type-I and type-II) are possible. The former is obtained by rotating a C–C bond of the sheet, while the latter is obtained by rotating a tilted B–C bond. The atomic configurations for the two types of SW defects in the BC_3 sheets along with the perfect configuration are shown in Fig. 4. The defect formation energy of the SW defects is defined as: $E_f = E_{pristine} - E_{SW}$, where E_{SW} and $E_{pristine}$ are the total energy of a BC_3 sheet containing a SW defect and that of a perfect sheet, respectively. Unlike the BN nanosheet [37], the SW defect in an *h*-BC_3 does not form unstable homoelemental

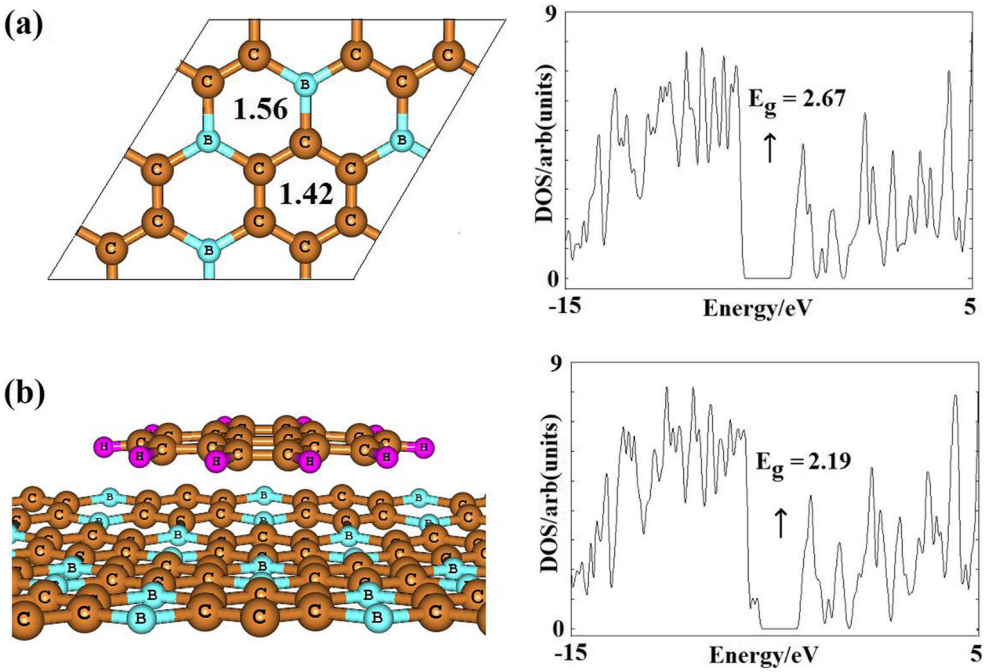

Fig. 2 Partial structure of optimized of (**a**) *h*-BC_3, (**b**) pyrene/*h*-BC_3 and their density of state (DOS) plot. Distances are in Å

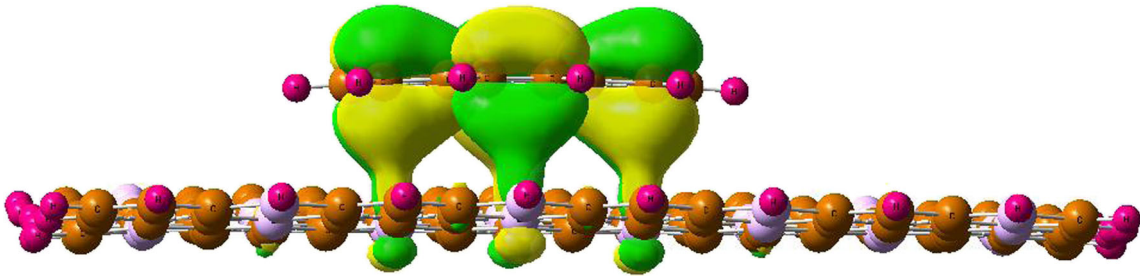

Fig. 3 HOMO profile of pyrene/*h*-BC_3

B-B bonds, and as a result, the structures are more stable. For SW defect type-I (SW-CC), the E_f is calculated to be about −259.2 kJ mol^{-1}, but that is found to be −349.5 kJ mol^{-1} for type-II (SW-BC). These negative values indicate that both of the defect formation processes are endothermic and also suggest that the SW-CC may be a more energetically favorable process than SW-BC. The main change in the pristine structure is that the bond belonging to the defect is compressed and stretched. Especially, the rotated C-C and B-C bond lengths are decreased to 1.35 and 1.50 Å, respectively.

Furthermore, the effect of the SW-defect on the adsorption behavior of pyrene was investigated. Different possible adsorption configurations of pyrene molecule being close to the defected site of the sheet are investigated. More detailed information from the simulation of the different pyrene/SW BC_3 sheets systems, including values of E_{ad}, electronic properties, and the charge transfer for these configurations, is listed in Table 1. As can be seen in Fig. 5 (SW-CC in panel a, SW-BC in panel b), after geometry optimization, it was found that three types of configurations are stable for each SW-defected sheet. In all of the configurations, the pyrene molecule was located on the top of the defected sites as parallel. Overall, the magnitude of the calculated E_{ad} exhibits the following order: **CC.1** (+167.7 kJ mol^{-1})>**CC.2** (+165.3 kJ mol^{-1})>**BC.3** (+164.6 kJ mol^{-1})>**CC.3** (+164.1 kJ mol^{-1})>**BC.2** (+162.9 kJ mol^{-1})>**BC.1** (+143.6 kJ mol^{-1}) with corresponding charge transfer of 0.218, 0.215, 0.214, 0.210, 0.206, and 0.183 electrons from the pyrene to the sheet. In order to interpret the pyrene interaction with the defected sheet, we drew plots of the HOMO for different pyrene/SW-defected sheets (Fig. 6). The results again indicate that similar to the pristine *h*-BC_3, the pyrene molecule undergoes the π-π interaction. Smaller E_{ad} of **BC.1** configuration than other complexes may be because of the lower overlap between π orbitals of the pyrene and the SW-defected sheet.

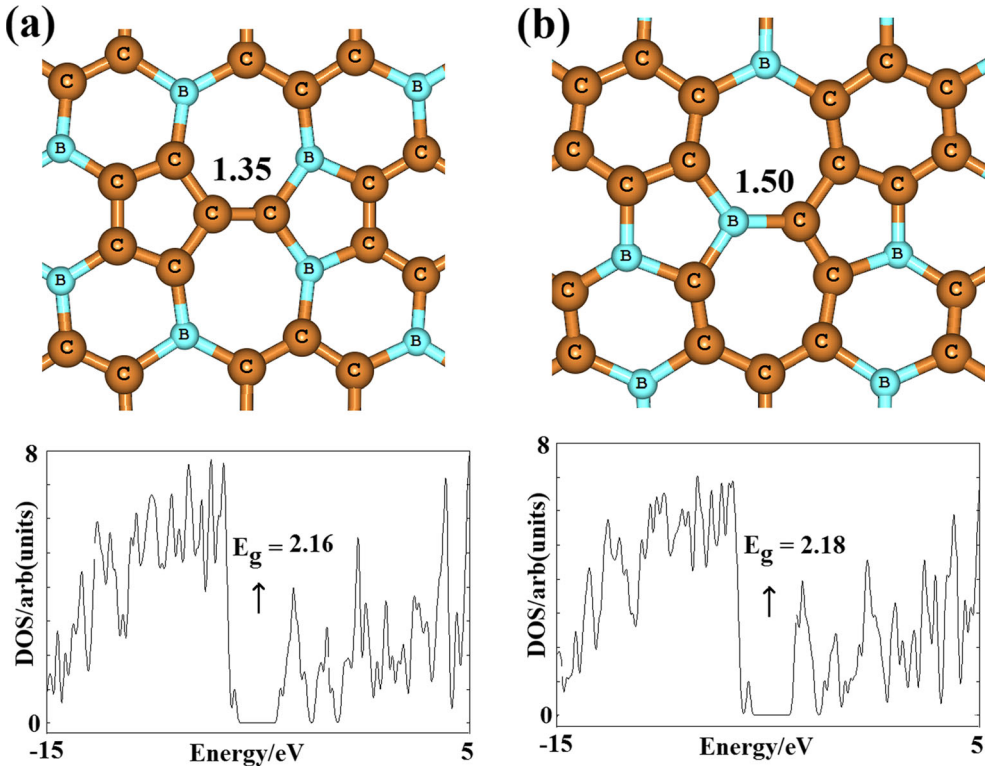

Fig. 4 Partial structure of optimized (**a**) SW-CC, (**b**) SW-BC and their density of state (DOS) plot. Distances are in Å

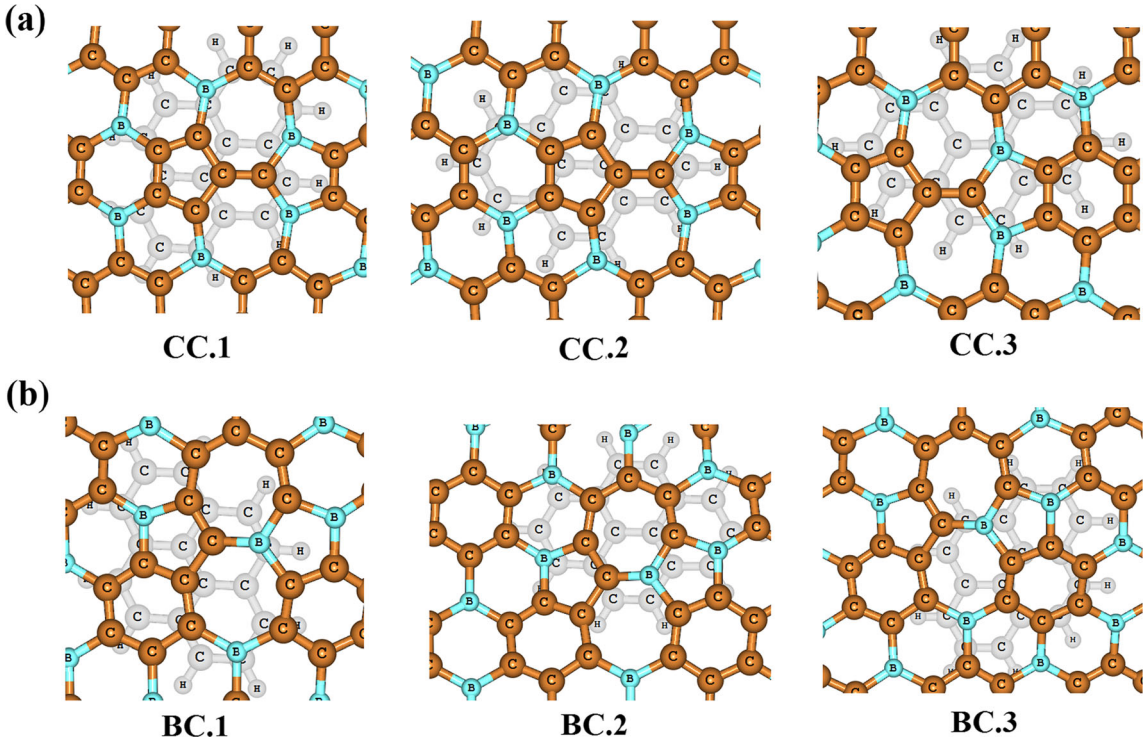

Fig. 5 Optimized structure of pyrene-functionalized (**a**) SW-CC, (**b**) SW-BC. Pyrene molecule is shown with gray color for better illustration

Electronic properties

Next, the influence of the pyrene adsorption on the electronic properties of the host sheet was investigated. As shown by the calculated DOS in Fig. 2a the pristine *h*-BC_3 is a semiconductor with an E_g value of 2.67 eV. After the SW formation, both conduction and valence levels slightly shift toward Fermi level, so the E_g of the sheet decreased from 2.67 eV in the pure *h*-BC_3 to 2.16 and 2.18 eV in SW-CC and SW-BC, respectively. Figure 4 (panels a and b) clearly shows that the SW-defected sheets are still a semiconductor. From Table 1, it can be seen that the HOMO and LUMO energies of the SW-defected BC_3 sheets have not changed significantly after the pyrene adsorption. However, after the pyrene adsorption on the pristine sheet, the valence level shifted to higher energies compared to the pure sheet, so the E_g decreased from 2.67 to 2.19 eV (Fig. 2b). It is well known that E_g (or band gap in bulk materials) is a major factor determining the electrical conductivity of a material and there is a classic relation between them as follows [38]:

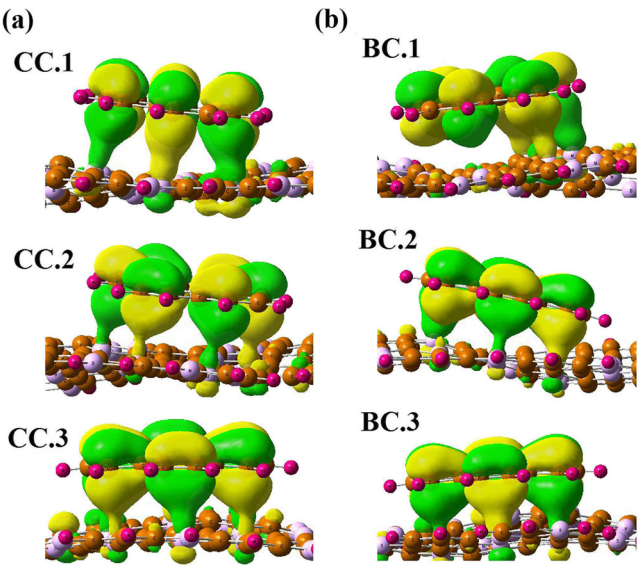

Fig. 6 HOMO profile of pyrene-functionalized (**a**) SW-CC, (**b**) SW-BC

$$\sigma \propto \exp\left(\frac{-E_g}{2kT}\right), \tag{2}$$

where σ is the electrical conductivity and k is the Boltzmann's constant. According to the equation, smaller E_g at a given temperature leads to larger electrical conductivity. Unlike the defected sheet, the considerable change of about 18.0 % in the E_g value demonstrates the high sensitivity of the electronic properties of pristine sheet to the pyrene adsorption.

Recently, there has been great interest in the field emission properties of graphene-like materials [39]. Graphene is currently of great interest in efficient field emission sources because of its unique electronic properties, large surface areas, sharp edges, and sustaining current densities. To further investigate the electronic properties of functionalized BC_3 sheets, we have studied the changes of work function of systems ascribed to the charge transfer between pyrene and the adsorbents. The work function of a semiconductor is the

least amount of energy required to remove an electron from the Fermi level to a point far enough not to feel any influence from the material. However, the emitted electron current densities in vacuum are theoretically described by the following classical equation:

$$j = AT^2 \exp\left(-\Phi \Big/ kT\right), \quad (3)$$

where A is called the Richardson constant (A/m^2), T is the temperature (K), and Φ (eV) is the material's work function. The Φ values were calculated using the following equation:

$$\Phi = E_{inf} - E_F, \quad (4)$$

where E_{inf} is the electrostatic potential at infinity and E_F is the Fermi level energy. In this consideration, the electrostatic potential at infinity is assumed to be zero. The work function changes (ΔΦ) were calculated by subtracting the work function of the clean BC_3 sheets from that of the corresponding adsorbed system. The results of Table 1 revealed that the Φs of the defected sheets remained almost unchanged after pyrene adsorption. In other words, the functionalization of SW-defected BC_3 sheets can be supposed as some kind of "*harmless modification*".

However, compared to the pristine BC_3 sheets (Φ= 1.33 eV), we note that the pyrene adsorption can significantly decrease the work function (Φ=1.09 eV). The reduction in the work function indicates that the field emission properties of the BC_3 sheets are facilitated after the adsorption of mentioned adsorbates. Furthermore, this results in reduced potential barrier of the electron emission for the *h*-BC_3, facilitating the electron emission from the sheet. Finally, it should be noted that further experimentally works are needed to support our results. Also, BC_3 sheets with larger sizes will give more exact results in comparison to our model. Saturating ends of the sheet with hydrogen atoms may affect its electronic properties. However, our concern was the change of electronic properties instead of absolute data.

Conclusions

The functionalization of the pristine and SW-defected BC_3 sheets with a pyrene was investigated theoretically. The HOMO profiles of functionalized sheet clearly proved that π-π stacking has a major contribution in the interaction. E_{ad} has been calculated to be in the range of 143.6 to 169.1 kJ mol^{-1}. After the pyrene adsorption, the E_g of the pristine sheet decreases, resulting in the electrical conductivity enhancement. Consequently, two types of SW defects for *h*-BC_3 labeled SW-CC and SW-BC are predicted. On comparison, SW-CC is more stable than SW-BC, energetically. In contrast to the pristine sheet, the pyrene functionalization results in little change in the electronic properties of SW-defected sheet. The pyrene functionalization modifies the work function of the BC_3 sheets and, as a consequence, the field-emission current densities of pyrene/BC_3 sheets may be significantly enhanced.

References

1. Novoselov KS, Geim AK, Morozov SV, Jiang D, Zhang Y, Dubonos SV, Grigorieva IV, Firsov AA (2004) Science 306:666
2. Sorkin V, Zhang YW (2011) J Mol Model 17:2825
3. Novoselov KS, Geim AK, Morozov SV, Jiang D, Katsnelson MI, Grigorieva IV, Dubonos SV, Firsov AA (2005) Nature 438:197
4. Rastegar SF, Peyghan AA, Hadipour NL (2012) Appl Surf Sci 265: 412
5. Peyghan AA, Noei M, Yourdkhani S (2013) Superlat Microst 59:115
6. Beheshtian J, Peyghan AA, Noei M (2013) Sens Actuators B: Chem 181:829
7. Beheshtian J, Soleymanabadi H, Peyghan AA, Bagheri Z (2012) Appl Surf Sci 268:436
8. Beheshtian J, Peyghan AA, Bagheri Z (2013) Struct Chem 24: 1565
9. Rastegar SF, Peyghan AA, Ghenaatian H, Hadipour NL (2013) Appl Surf Sci 274:217
10. Geim AK, Novoselov KS (2007) Nat Mater 6:183
11. Meyer JC, Girit CO, Crommie MF, Zettl A (2008) Appl Phys Lett 92: 123110
12. Son YW, Cohen ML, Louie SG (2006) Phys Rev Lett 97:216803
13. Tanaka H, Kawamataa Y, Simizua H, Fujitaa T, Yanagisawaa H, Otanic S, Oshima C (2005) Solid State Commun 136:22
14. Tomanek D, Wentzcovitch RM, Louie SG, Cohen ML (1988) Phys Rev B 37:3134
15. Wang Q, Chen LQ, Annett JF (1996) Phys Rev B 54:R2271
16. Pontes RB, Fazzio A, Dalpian GM (2009) Phys Rev B 79:033412
17. Ding Y, Wang Y, Ni J (2009) Appl Phys Lett 94:073111
18. Ding Y, Ni J (2009) J Phys Chem C 11 3:18468
19. Shiral Fernando KA, Lin Y, Sun YP (2004) Langmuir 20:4777
20. Shan C, Yang H, Han D, Zhang Q, Ivaska A, Niu L (2009) Langmuir 25:12030
21. Chełmecka E, Pasterny K, Kupka T, Stobi ń ski L (2012) J Mol Model 18:2241
22. Lemek T, Mazurkiewicz J, Stobinski L, Lin HM, Tomasik P (2007) J Nanosci Nanotechnol 7:3081
23. Moradi M, Noei M, Peyghan AA (2014) Struct Chem 25:221
24. Zhou J, Wang Q, Sun Q, Jena P (2011) J Phys Chem C 115:6136
25. Vijayaraghavan V, Garg A, Wong CH, Tai K, Bhalerao Y (2013) J Nanostruct Chem 3:83
26. Garg A, Garg A, Tai K (2014) Comput Geosci1 8:45
27. Garg A, Garg A, Tai K, Sreedeep S (2014) Eng Appl Artif Intell 30: 30
28. Vijayaraghavan V, Garg A, Wong CH, Tai K, Mahapatra SS (2014) Measurement 50:50
29. Garg A, Vijayaraghavan V, Wong C, Tai K, Gao L (2014) Sim Model Pract Theo 44:1
30. Schmidt MW, Baldridge KK, Boatz JA, Elbert ST, Gordon MS, Jensen JH, Koseki S, Matsunaga N, Nguyen KA, Su S, Windus TL, Dupuis M, Montgomery JA (1993) J Comput Chem 14:1347
31. Grimme S (2004) J Comput Chem 25:1463
32. O'Boyle N, Tenderholt A, Langner K (2008) J Comput Chem 29:839

33. Moradi M, Peyghan AA, Bagheri Z, Kamfiroozi M (2012) J Mol Model 18:3535
34. Beheshtian J, Peyghan AA, Bagheri Z (2012) J Mol Model 19:391
35. Beheshtian J, Baei MT, Peyghan AA, Bagheri Z (2012) J Mol Model 18:4745
36. Peyghan AA, Moradi M (2014) J Mol Model 20:2071
37. Li Y, Zhou Z, Golberg D, Bando Y, Schleyer PVR, Chen Z (2008) J Phys Chem C 112:1365
38. Ahmadi Peyghan A, Hadipour N, Bagheri Z (2013) J Phys Chem C 117:2427
39. Asaka K, Nakayama T, Miyazawa K, Saito Y (2012) Carbon 50:1209